Master Thesis, Department of Geosciences

Receiver function analysis

Seismic imaging of the crust beneath TROLL seismic station in Queen Maud Land, Antarctica

Andreas Torsvik

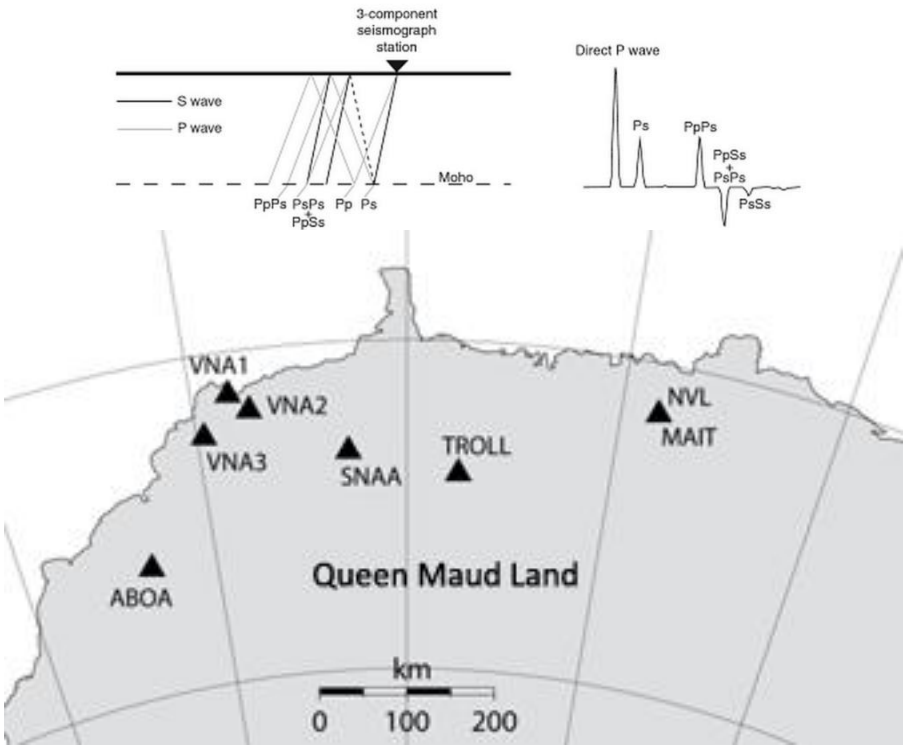

UNIVERSITY OF OSLO

FACULTY OF MATHEMATICS AND NATURAL SCIENCES

-

Receiver function analysis

Seismic imaging of the crust beneath TROLL seismic station in Queen Maud Land, Antarctica

Andreas Torsvik

Master Thesis in Geosciences

Discipline: Geophysics

Department of Geosciences

Faculty of Mathematics and Natural Sciences

University of Oslo

01.06.2015

-

Acknowledgment

I would first of all like to thank my supervisors Johannes Schweitzer (NORSAR) and Valerie Maupin (University of Oslo) for guidance and advise related to the study. In addition, I would like to thank NORSAR for providing me with office space and necessary resources. Also, I would like to thank Charles J. Ammon (Penn State University) for providing the computer programs used to generate and process the receiver functions.

Andreas Torsvik

Oslo, 2015

-

Abstract

In this this study, receiver function analysis of the crust underneath TROLL seismic station in Queen Maud Land, Antarctica was performed. An analysis of the neighboring seismic station SNAA was carried out as well to provide ground of comparison.

Receiver function analysis is a seismic method utilizing that fact that teleseismic P-waves encountering a subsurface boundary at particular angels of incidence will result in refracted and reflected P and S-waves. The generated waves of interest are those resulting from the local structure underneath the receiver, and by deconvolution and source equalization, these local effects can be isolated into a data series known as the receiver function. An estimate of the local velocity-structure model can then be computed through an iterative process of forward modeling and inversion. Throughout this study, the receiver function analysis is carried out in a step-by-step manner; from raw three component seismograms to estimated structure model. In addition, crustal depth and $V_P V_S$ ratios were estimated through the method of H-κ analysis.

Computation programs made available by Charles Ammon were used for the processing. The programing codes are a collaboratively written by Tom Owens, George Randall, George Zandt, and Charles Ammon. In addition, the Seismic Analysis Code (SAC) program was used along with auxiliary SAC programs provided by George Helffrich.

The crustal thickness beneath the TROLL seismic station was modeled to be approximately 42.5 km thick. The confidence in this result is further supported by similar studies conducted at surrounding seismic stations.

-

Table of contents

-

List of figures of figures

-

1 Introduction

In this this study, receiver function analysis of the crust underneath two seismic stations is to be conducted. Receiver function modeling is a seismic method utilizing teleseismic waves.

The workflow of the analysis can be summed up in the following way;

- Data extraction
- Data preparation
- Deconvolution and source equalization (response isolation)
- Forward modeling and inversion
- Final model

Each process will be explained in detail throughout this thesis. To supplement the receiver function analysis, H-κ analysis will be performed to estimate bulk crustal structure parameters.

1.1 Geological setting

The areas of investigation for this study will be the crustal structure below two seismic station in the Antarctic. Both stations are located in Queen Maud Land, which is a Norwegian territory positioned in East Antarctica, limited longitudinally between 20°west and 45°east (Norwegian Polar Institute, 2015). Most of the territory is covered by the Antarctic ice sheet, and along the coast, there is no ice-free land. Within the territory however, some 150-200 km from the coast, numerous rocky peaks from mountain ranges breach the ice (Gjeldsvik, 2009).

The major geological units of today's Queen Maud Land, or East Antarctica as a whole, can roughly be divided into three main groups: (1) bedrock composed of Precambrian gneiss, (2) mountain ranges of Cambrian crystalline and granite, and (3) Jurassic sedimentary and volcanic layers found mostly in the western parts Queen Maud Land (Kaul et al., 1991; Elliot 1991). These geological units were predominantly formed by three tectonic events. The Precambrian gneiss formation is associated with the formation of the supercontinent Rodinia, caused by the Grenville orogeny (1.1 Ga) which was a long-lived Mesoproterozoic mountain-building event (Jacobs et al., 2003). The crystalline and granitic composition of the mountain region in the central areas of Queen Maud Land are the result of the Pan-African orogeny (500-600 Ma),

which was the driving force of the formation of the supercontinent Gondwana (Elvevold, 2005). Finally, the breakup of Gondwana (160 Ma), which originated in the ocean basin off Queen Maud Land, resulted in the younger sedimentary and volcanic rocks found mostly the western parts of the territory (Jacobs et al., 1996).

1.2 Seismic Stations

1.2.1 TROLL Station

In February 2012, NORSAR (Norwegian Seismic Array) installed a permanent seismic broadband station at the Norwegian research base Troll in Antarctica. The research station is located at 72.01° S, 2.53° E, approximately 235 km from the coast, at Jutulsessen in Queen Maud Land (Figure 1). The seismic station is named TROLL, and it extends the network of permanent seismic stations in Queen Maud Land already in place. Former stations have however often been installed on the ice shield, whereas the TROLL station is installed directly on a bedrock prominence on top of a hill at 1399 m above sea level. This element greatly improves signal quality in favor of the TROLL station, as glacial movement as well as unwanted signal reflections from the bottom of the ice layer affects stations situated on ice. Three-component (vertical, north-south, and east-west) measurements of ground movements are recorded continuously in the frequency range of 1 mHz up to 48 Hz with a maximum sampling rate of 100 Hz (Schweitzer et al., 2013). The station has been operational since February 5th, 2012, with only minor interruptions.

-

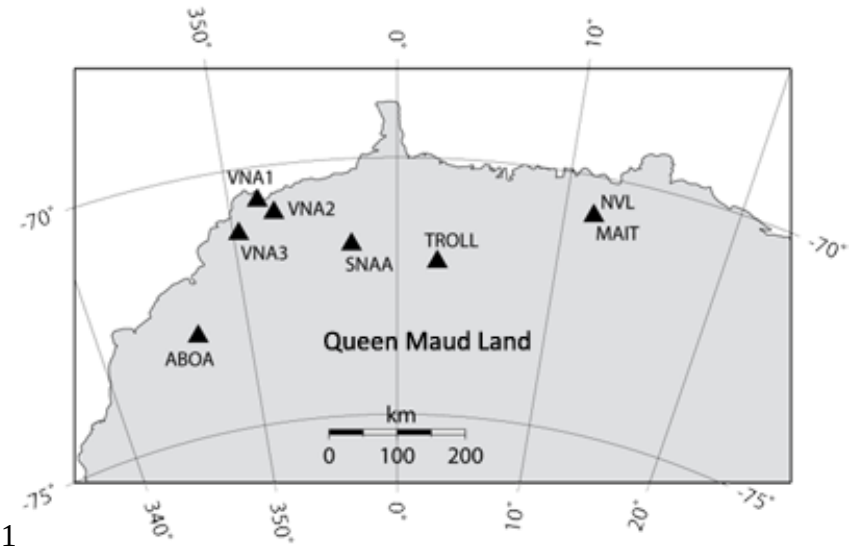

1

Figure 1 - Map of seismic stations located on Queen Maud Land (courtesy of NORSAR).

1.2.2 SNAA Station

The closest neighboring seismic station to TROLL is Sanae (SNAA), also located directly on bedrock. The SNAA station is a part of the research initiative by the South African National Arntartic Program (SANAP), and is located at 71.67° S, 2.84° W, at an elevation of 846 m above sea level, on top of Vesleskarvet in Queen Maud Land. This station has been operational since December 1997 and is considered among the best performing three- component stations of the International Monitoring System (IMS). A comparison study of detection capability between the TROLL and SNAA stations has been conducted by NORSAR to evaluate the performance of the TROLL station (Schweitzer et al., 2013). From the analysis of six months' worth of data, the detection capability of TROLL was estimated to be 0.1 – 0.2 units of magnitude better than SNAA for teleseismic events (20° - 90° and 115° - 180°). Bearing in mind that the SNAA station is considered among the best performing stations of the IMS, and that the TROLL station is considered even better, then data from the two stations may be well suited for performing seismic imaging using teleseismic events.

2 Receiver function method

The receiver function method is a powerful technique for imaging the crustal and upper mantle characteristics of the Earth (at a local level). The basic idea of the receiver function method is that teleseismic waveforms contain information that can be used to predict and investigate crustal structures underneath seismic stations. In order to understand the receiver function method, some basic knowledge about the Earth's structure and seismology has to be introduced.

2.1 Basic Seismic

2.1.1 Structure of the Earth

In reality, the Earth has a shape that approximates an oblate spheroid, and a complex structural interior that can be divided and subdivided into numerous layers defined by mechanical or chemical properties. However, for the purpose of this thesis, a simpler understanding of the Earth model is sufficient. In short, the Earth is a spherical structure with a mean radius of 6371 km, with stratified layering characteristics such as an onion. The three major structural layers are the crust, mantle and core.

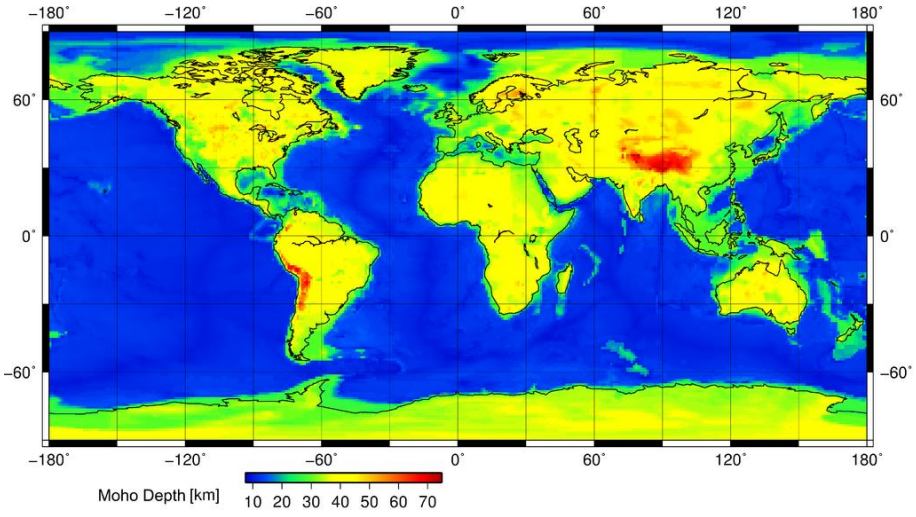

Figure 2 - Geophysical map showing the position of the Moho discontinuity across the Earth (courtesy of Christian-Albrechts University of Kiel)

In particularly important to the receiver function method is the boundary between the crust and mantle. This boundary was first found in 1909, and is called the Mohorovičić discontinuity (Moho), named after the Croatian seismologist who discovered it (Mohorovičić, 1909). The

-

depth of the Moho varies greatly depending if it is located below oceanic crust or continental crust (Figure 2). The Moho below the ocean floor ranges from 5 to 10 km, while the depth below the continents ranges from 20 to 70 km, with an average of 35 km (Monroe, 2008).

2.1.2 Seismic Event

For the purposes of this thesis, a "seismic event" is referring to an earthquake. An earthquake is in simplest form defined as a sudden movement of the Earth's crust. The coordinate location of the earthquake is called the *hypocenter*, while the, perhaps more familiar term, *epicenter* refers to the origin location projected on to the Earth's surface. The sudden movement that occurs during an earthquake is in reality a sudden release of energy. This energy propagates through and along the structures of the Earth as seismic waves. The seismic waves can be divided into three groups: *body waves* that travel through the interior of materials, *surface waves* that travel along surfaces or interfaces, and *normal modes*. Only body waves are of value to the receiver function method, thus further explanation of surface waves and normal modes is unnecessary.

2.1.3 Body Waves

Body waves are divided into Primary waves (P-waves) and Secondary waves (S-waves). P-waves are compressional waves that produce displacement in the direction (longitudinal) of wave propagation. S-waves are shear waves producing displacement perpendicular to the direction (transverse) of wave propagation (Stein and Wysession 2003). The perpendicular displacement cannot occur within fluids, thus S-waves can only travel through solid material, whereas P-waves can travel through both solid and liquid materials. Furthermore, P-waves travel faster than S-waves; the velocity of the S-wave is typically around 60% of that of P-waves in any given material, but varies depending on material composition. As a result of this difference in velocity, the P-wave will be the first arriving wave on a seismogram. An example of a seismogram is shown in Figure 3. The seismogram represents measurement of the ground movement by a seismometer recorded as a time series. For a three-component seismic station, movements are measured and recorded in three directions: east-west (E), north-south (N), and vertical (Z).

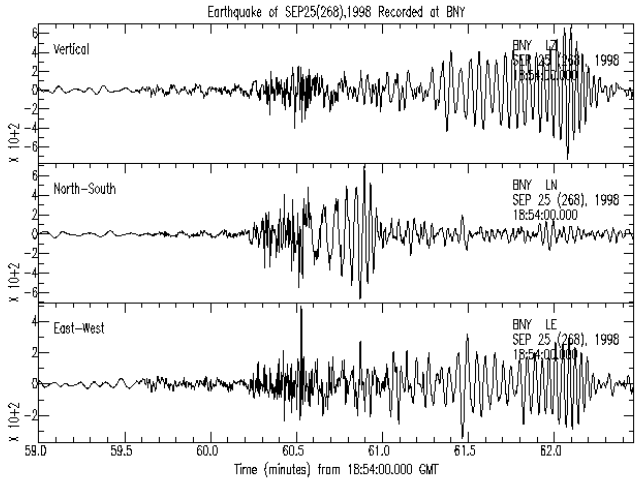

Figure 3 - A three component seismogram (Courtesy of IRIS)

2.2 Receiver Function Method

2.2.1 The receiver function

Receiver functions are time series, computed from three component seismograms, which shows the relative response of Earth structure near the receiver. These responses originate from the different paths traveled by waveforms from teleseismic waves. When a propagating body wave hits an interface, the waveform's energy is transmitted, reflected, and possibly converted, depending on the properties of the interfacing materials and the incident angle of the wave. The Moho is an example of such an interface, specifically a solid-solid interface as it is the boundary between solid mantle and core. As a P-wave travels up through the mantle and hits the Moho, most of the waveform will continue transmitted as a P-wave, while some part of the waveform will be converted and transmitted as an S-wave. These waves arrive at the seismic station as responses identified as the *Direct P wave* and *Ps* (Figure 4). In addition, some of the initial waveform is "lost", as it is reflected back down into the mantle as P and S-waves; these waves are for the receiver function method not considered. Reflections that are to be considered however, are the reflections occurring at the free surface (crust-air interface). The reflection of the transmitted P-wave at this interface can cause *multiples* (*PpPs*, *PsPs*, *PpPs*) which are wave signals reflected back up from the Moho interface (Figure 4).

-

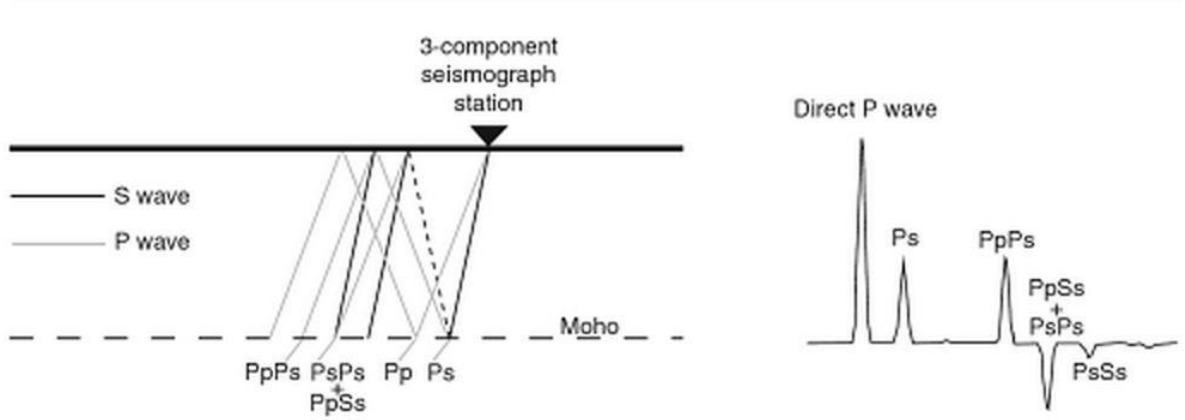

Figure 4 - Receiver function analysis of Earth structure beneath a seismograp station (left). The arrivals, and subsequent reverberations, can be isolated by receiver function analysis (right). Modified by Ammon (1991). (Courtesy of Hellfrich et. al, 2013)

2.2.2 The receiver function technique

Of the terms briefly explained above, there are three key concepts that form the basis of the receiver function method:

- P to S conversion at the crustal boundary
- Difference in velocity of P-waves and S-waves
- Multiples

The basic idea of how these concepts are of value can be described through the example as illustrated above (Figure 4); a waveform arriving at a seismic station above a single layer (crust). P-wave signals from distant seismic events (earthquakes) are converted to S-waves (Ps) at the Moho. As S-waves travel slower than P-waves, these signals will have a longer travel time through the crust, and will therefore arrive later at a seismic station than a direct P-wave. The difference in arrival time between the direct P-wave and Ps can, if provided a velocity model, give a direct calculation of the depth of the interface (in this case, the Moho). Furthermore, the multiples (PpPs, PsPs PpSs) contain further information and provides redundancy, which further strengthen ssubsurface estimations. The main goal of to the receiver function method is that the near-receiver structure must be isolated from the source and distant structure effects. The technique for doing so is further explained in chapter 4, section 1 (4.1).

3 Data Selection and Preparation

3.1 Retrieving events

3.1.1 Event selection

Several million earthquakes occur in the world each year. There are however a few criteria that needs to be met in order for the earthquakes to be beneficial for imaging purposes. First, a certain signal strength is required; this is dependent on the magnitude of the earthquake. Secondl, the event epicenter must be within a certain distance interval from the seismic station in order to get propagation paths resulting in signal arrivals usable for the receiver function method (wave propagation through the mantle and crust, resulting in P-S conversions). These waves are called teleseismic waves, and are for P-waves defined as waves originating from earthquakes at a radial distance farther than 30° (Rondenay, 2009). For the purposes of this thesis, only events with body wave magnitude greater than 6 mb, occurring at epicentral distances between 30° and 95° from a seismic station, were considered suitable events.

The International Seismological Center (ISC) provides the public with full access to data within the ISC Bulletin. The ISC Bulletin database contains data contributed by seismological agencies from around the world. The data includes information about seismic events such as hypocenters, phase arrival-times, and amplitudes. On their website, it is possible to perform customized event catalogue searches within this database (ISC, 2015). The search parameters were set to only include events with a minimum magnitude of 6 mb, and the time period of the search was set to the start date of operation for the individual station (TROLL and SNAA) up until 22th January, 2015. In terms of regional search criteria, the website offers circular searches from a given coordinate based on an input radius. It does however not include the option of a circular interval search. In order to retrieve events occurring only within the desired distance interval from the seismic stations (30° to 95°) two separate searches were performed: one at a radius of 95°, and the other at 30°. The outputted event lists were then compared and the events in common were removed, leaving only events with epicentral distances between 30° and 95°.

-

3.1.2 Events TROLL

For the TROLL seismic station, 154 events met the criteria. However, meeting the initial criteria of magnitude and epicentral distance does not necessarily mean the events are useful for imaging purposes. To identify and remove undesirable events, a quick-and-dirty process of visual filtering was performed. The NORSAR Event Processing (EP) System was used to extract and view the seismograms for each of the 154 events. The events were evaluated by the amount of noise present, and by how easily identifiable the onset of the direct P-wave arrival were on the seismograms. 60 events were deemed to have either considerable amounts of noise, or difficulties of identifying waveform arrivals. An example of such a bad event is shown in Figure 5, while a good event is shown in Figure 6. The bad events were removed from the data list, leaving 94 events for further processing.

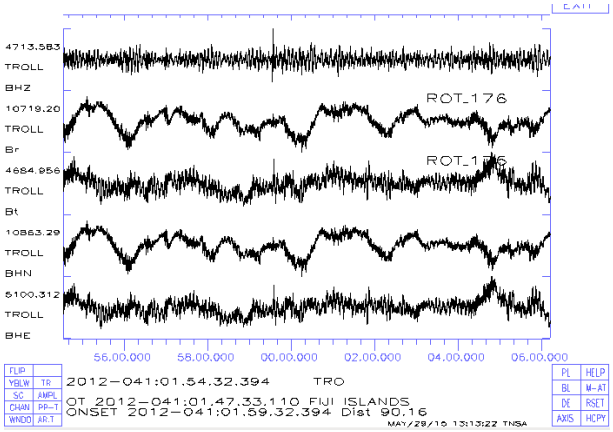

Figure 5 - Example of a poor event

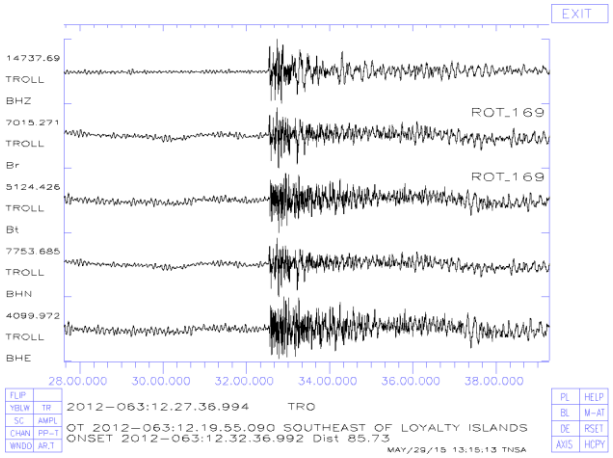

Figure 6 - Example of a good event

Figure 7 shows a distribution map of these 94 events. The plot was created using the Generic Mapping Tools (GMT) software. As can be seen on the plot, the distribution of events is rather scarce for some areas. Figure 8a) and b) shows diagrams which further demonstrates this, as particular radial distances and azimuths, has little to no earthquake occurrences.

3.1.3 Events SNAA

685 events met the magnitude and epicentral distance criteria for the SNAA station. The same manual filtering process was performed on this data set by viewing the seismogram with the EP software. Similarly to the TROLL data set, approximately 40% of the events were considered undesirable; 285 events were removed, leaving 400 events for further processing. An event distribution plot has been created for these events (Figure 9). As with the TROLL station, the coverage of events is somewhat scarce for the SNAA station as well; the number of events is greater, but the events are rather clustered. There are in particular three apparent chains of earthquake occurrences, which is associated with the "Pacific Ring of Fire". This clustering of events can further be seen in the diagrams in Figure 10a) or b). This distribution of events is though to be expected, as about 90% of the world's earthquakes and 81% of the world's largest earthquakes occur along the Ring of Fire (USGS, 2015).

-

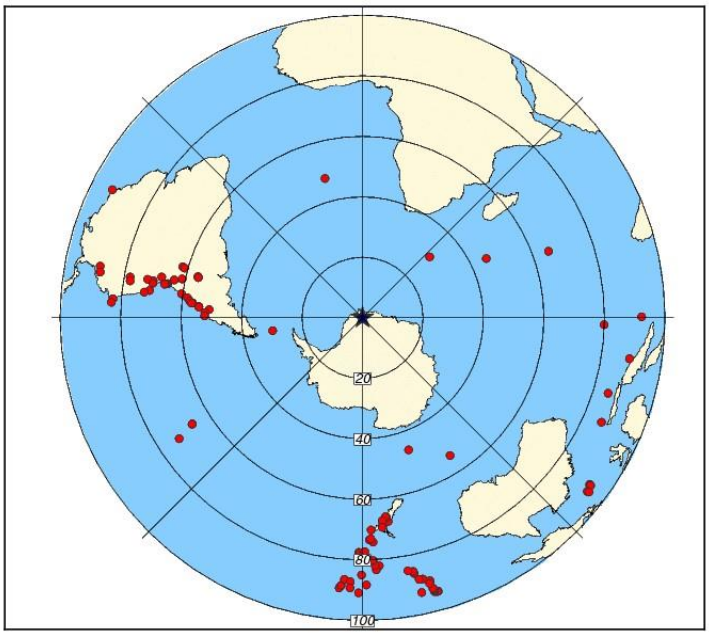

Figure 7 - Event distribution map for TROLL seismc station

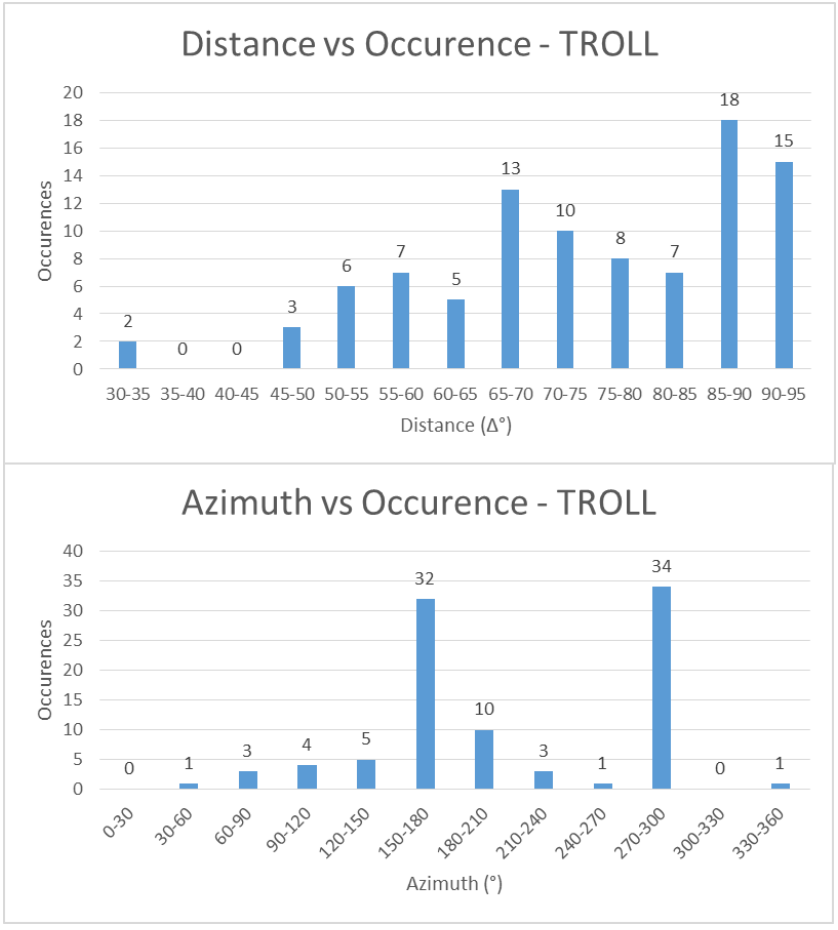

Figure 8a) - Distance vs Occurence plot for TROLL. 8b) - Azimuth vs Occurence plot for TROLL.

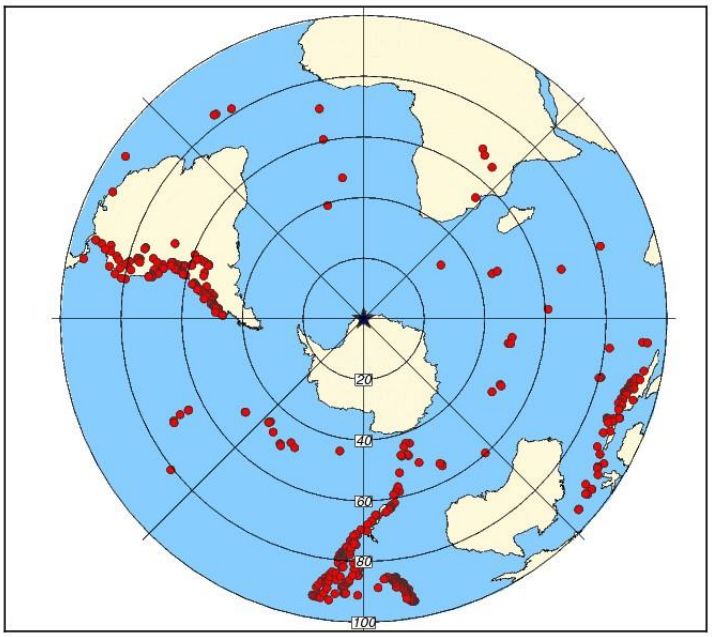

Figure 9 - Event distribution map for SNAA seismic station

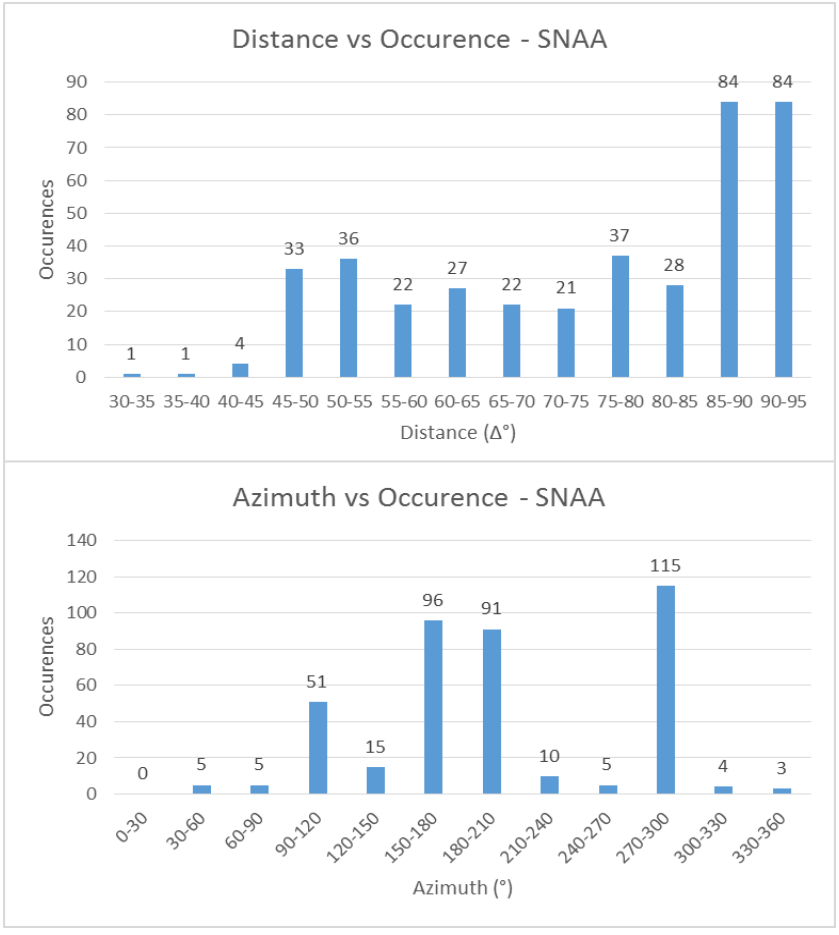

Figure 10a) - Distance vs Occurence plot for SNAA. 8b) - Azimuth vs Occurence plot for SNAA.

-

3.2 Data preparation

The events considered good enough for further processing were extracted from NORSAR's database using the EP software. Broadband channel data was retrieved at 40 Hz for TROLL and 20 Hz for SNAA. The band data consists of three separate files, corresponding to the three components: vertical motion (BHZ), east-west motion (BHE), and north-south motion (BHN). The file format for these files were MiniSEED.

3.2.1 MiniSEED to SAC

The programs used in this study takes use of the Seismic Analysis Code (SAC) format. Thus, in order to continue the processing, a file conversion had to be performed. A conversion script called "mseed2sac" was downloaded from IRIS (Trabant, 2013). The software converts Mini-SEED waveform data to SAC format as either ASCII or binary output. The programs provided by Ammon accepts binary only, so this file format was selected.

3.2.2 Editing Header Values

The SAC file format consists of a header that describes the trace (also known as metadata) and a section that contains actual data for the seismogram (Hellfrich et al., 2013). The header includes information such as time and sampling of the signals, and can contain information about the location of the station and event. In order for the SAC software to rotate the horizontal seismogram (BHN and BHE) into the theoretically based radial and tangential directions needed for the receiver function analysis, the files need to contain information about the position of the event and the station in question. The extracted files does not include the positional information for either the event or station. A macro was written to write the appropriate coordinate information into the header of each event.

3.2.3 Pre-Processing

The waveforms themselves are at this point still raw observations (Figure 11). Prior to computing the receiver functions, the data needs to be processed.

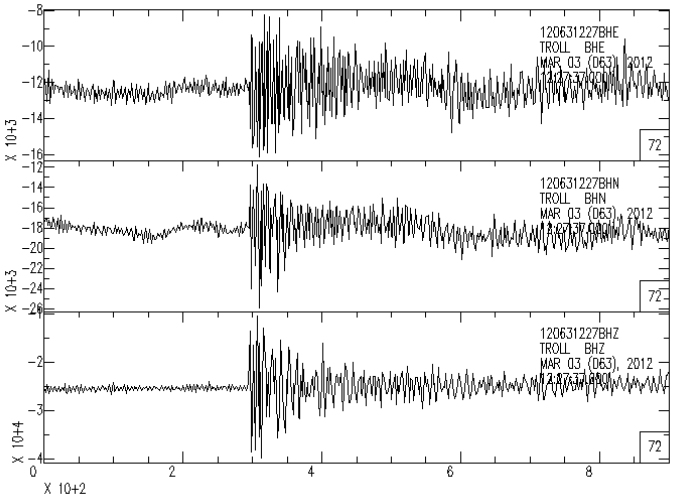

Figure 11 - Raw three component seismogram for an event recorded at TROLL seismic station

The data was edited using SAC commands written as a macro. First, the reference times for the three components BHZ, BHE and BHN were synchronized. The approximate P-onset was interactively picked using the plot and pick command (PKK), and the data was cut 60 s before and 60 s after the P-onset using the cutting command. Mean and trend were removed from the observation and to window the function, and a cosine taper was applied on the left and right fifth of the signal. The possible differences in component instrument gains were neglected as it assumed to be very low. Some of the programs to be used for the receiver function analysis have limitations as to how many points of data each processed file can contain. Windowing the data through the cut command greatly reduced the number of points already, but in order to reduce the number of points further, the data had to be downsampled. The downsampling of the data was performed by the use of the decimate command. Initially, the data from TROLL was at 40 Hz and SNAA at 20 Hz, so decimation was applied such that the sampling rate was 10 Hz for both sets of data. The raw seismogram data (Figure 11) is shown in its pre-processed form in Figure 12. The seismograms have been shifted to a zero-amplitude reference line, the data has been window to a shorter time interval, and the signal appear to be less noisy.

-

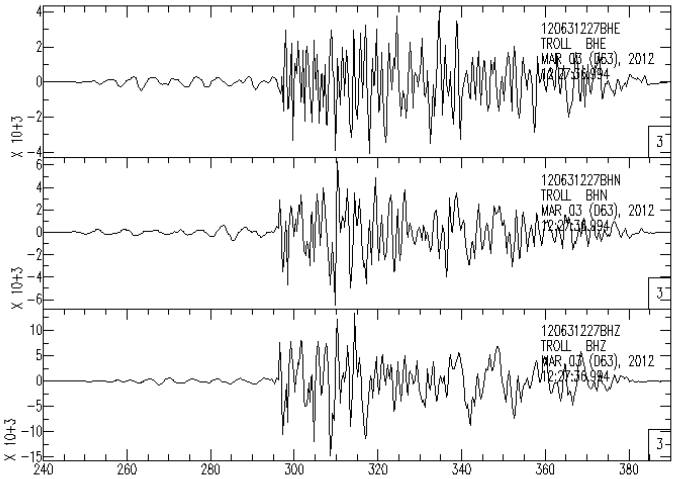

Figure 12 - Pre-processed three component seismogram recorded from TROLL seismic station

3.2.4 Rotation

So far, the seismic data is still in the original ZNE coordinate system; vertical, north-south, and east-west. In this rotation system however, the data is not aligned in the axis between the station and the earthquake; thus energy from the various types of seismic waves are registered in each of the horizontal components. In order to better isolate the energy from the different wave types, a two-dimensional rotation is applied. The vertical component (Z) remains the same, while the two horizontal components are rotated into the radial (R) and tangential (T) components through the following equation:

$$\begin{bmatrix} R \\ T \\ Z \end{bmatrix} = \begin{bmatrix} -\cos\gamma & -\sin\gamma & 0 \\ \sin\gamma & -\cos\gamma & 0 \\ 0 & 0 & 1 \end{bmatrix} \begin{bmatrix} N \\ E \\ Z \end{bmatrix} \quad (1)$$

Where N, E, Z are the original north-south, east-west, and vertical components respectively, and γ is the back-azimuth of the incident wave. This rotates the horizontal data such that the component will be directed along the angle given by the station-event back-azimuth plus or minus 180 degrees. The radial component therefore points from the event toward the station, and the transversal component points perpendicular to that (Figure 13). The SAC program was used to perform the rotation for all horizontal data components.

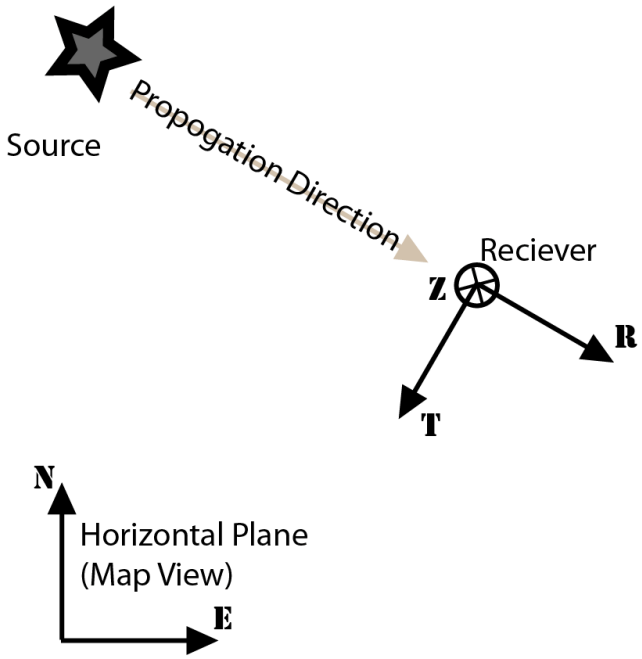

Figure 13 - Illustration of the orientation of the ZRT system relative to the ZNE system (Courtesy IRIS)

In terms of isolation of wave types, this approach assumes near-vertical incidence of waves such that P-waves are confined to the vertical component while the converted S-waves are contained in the radial component. In reality, the incident waves have considerable incidence angles, which causes some signal leakage between the components. However, the assumptions are acceptable to first order and have been widely employed in teleseismic imaging studies (Rondenay, 2009). In order to further isolate the waveform energies, the coordinate system LQT could be employed. This is a three dimensional system which in addition rotates the ZRT components in the direction of polarization of the incident P-wave (Plešinger et al., 1986). This coordinate system was however not considered, as the programs used to isolate the receiver response require input in the ZRT system.

-

4 Processing

4.1 Deconvolution

The earliest receiver function studies such as Phinney (1964) worked in the frequency domain using the ratio of amplitude spectra to estimate the gross characteristics of structure. The works of Clayton and Wiggins (1976) extended the method to include water-level-stabilization and phase information by using a complex frequency-domain ratio and inverse transforming back into the time domain. Langston (1979) continued the advancements further and moreover developed a source equalization procedure to remove the effects of near-source structure and source time functions. For this study, an iterative time-domain deconvolution approach is used; following the method of Ligorría and Ammon (1999). This technique is an adaption of the work by Kikuchi and Kanamori (1982) who proposed a method to estimate far-field source time functions. Advantages of using this technique over other deconvolution techniques in the frequency domains is first of all that that the time-domain iterative approach requires no choice of optimal stabilization parameters such as water-level, damping or time-domain smoothing. Secondly, the iterative approach is causal, such that it is easy to identify receiver functions that cannot satisfy the defining convolution equation (2).

There is a convolutional relation between the vertical and radial components of motion. The receiver function $E_{R_i}(t)$, is related to the radial $R(t)$, and vertical $Z(t)$ components through the equation:

$$R(t) = Z(t) * E_{R_i}(t) \qquad (2)$$

The foundation of the iterative deconvolution approach is a least-squares minimization of the difference between the observed horizontal seismogram and a predicted signal generated by the convolution of an iteratively updated spike train with the vertical-component seismogram (Ligorría and Ammon 1999). The vertical component *Z(t)* is first cross-correlated with the radial component *R(t)* to estimate the lag of the first and largest spike in the receiver function. Then the convolution of the current estimate of the receiver function $E_{R_i}(t)$ and the vertical-component seismogram is subtracted from the radial-component seismogram; $R(t) - E_{R_i}(t) * Z(t)$. Throughout the iteration, the misfit between the vertical and receiver-function convolution and the radial component seismogram is reduced, and the iteration halts when the

reduction in misfit with additional spikes becomes insignificant. The output of this algorithm is the receiver function, containing the estimated spike lags and amplitudes.

The programs takes use a normalized Gaussian filter, and is used to get rid of high frequency noise in the receiver functions. The filter is defined as follows:

$$G(\omega) = e^{-\frac{\omega^2}{4a^2}} \qquad (3)$$

Where ω is the radial frequency ($2\pi f$), and a is the Gaussian width factor. Several values of the Gaussian width factor was tested. A width factor of 2.5 or above resulted in noisy receiver functions, while a width factors less than 1.0 produced receiver functions where the spikes of interest had been compromised. A width factor of 1.5 was evaluated to be the best fit for the data, which is a value recommended by others conducting similar studies (Ligorría and Ammon 1999; Midzi and Ottermöller, 2001; Minoo, Kosarian 2006). In time domain, this width factor corresponds to an approximate 1.36 s pulse width.

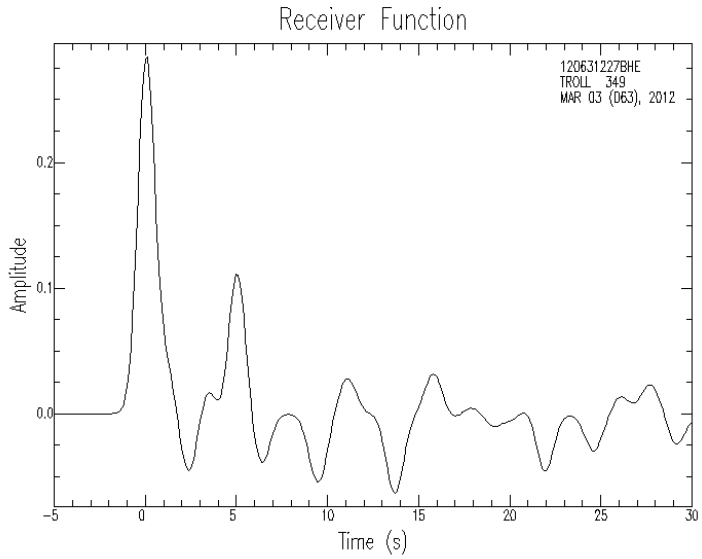

Figure 14 - Resulting receiver function for an even from TROLL seismic station

The observed vertical and radial component of each event was processed. The computations was set to iterate 200 times, or until converging of the solution. To be able to evaluate the result of the deconvolution, the misfit between the radial seismogram and the final receiver function estimate convolved with the observed vertical component was computed. This misfit value was used to identify poor events not suited for further investigation. Only deconvolutions resulting in a receiver function reproducing more than 90% of the signal was accepted. Solutions that did

-

not meet the 90% criteria was removed; leaving 34 and 171 receiver function estimates for TROLL and SNAA respectively. A resulting receiver function seismogram for an event from TROLL station is plotted in Figure 14.

4.2 Stacked Receiver Function

As the subsurface of the Earth is far from homogenous, the waveform travel from epicenter to receiver station is different for all the seismic events. As a consequence, all the generated receiver function estimates from deconvolution will provide unique solutions. To illustrate this uniqueness, receiver function estimates for two events recorded at TROLL station are compared in Figure 15. Differences between the receiver functions can be observed, but for the most part they are very similar. This is for modelling purposes a good sign, as this indicates responses created by a similar subsurface. If a subsurface is more complex with greater structural variations, the effects of difference in wave incidence angle and incidence azimuth will be greater. In order to improve the receiver function representation for a given seismic station, the available receiver function from observations are summated to increase the signal-to-noise ratio. This summation procedure is called signal stacking.

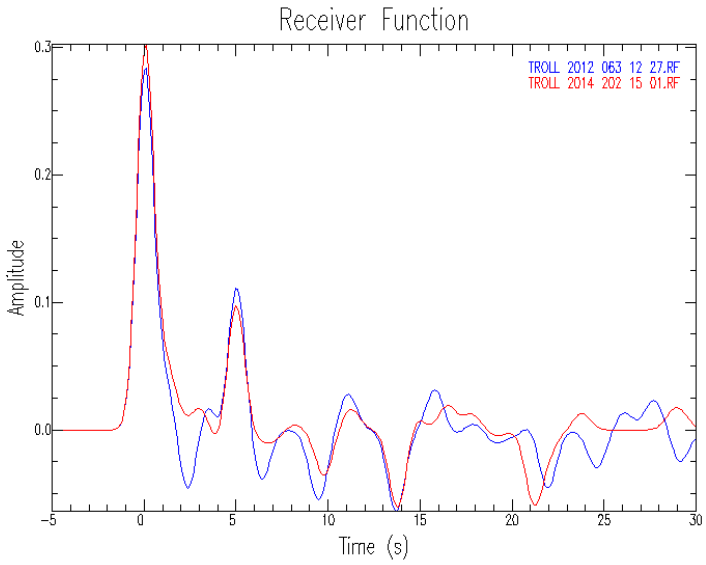

Figure 15 - Comparison of two receiver functions from TROLL seismic station.

The SAC software contains the Signal Stacking Subprocess (SSS). The subprocess is among several things, designed for combining traces for graphical display and for stacking data to suppress noise and enhance signal (Hellfrich et al., 2013). The receiver function traces are read in and added to a stack. In order to view the traces of a stack, or to sum all the traces within a

stack, a time window must be defined. The time window was defined from -5 to 30 s, as this sufficiently includes the signal responses of interest. The range variable is by standard set to be the distance between station and event, and the unit can be either degrees or kilometers. For plotting purposes however, this variable can be reallocated to any other paramter in the SAC header file by the use of the *changestack* command. Figure 16 shows the plot of the TROLL stack file list in a record section format; plotted with time and epicentral distance in degrees.

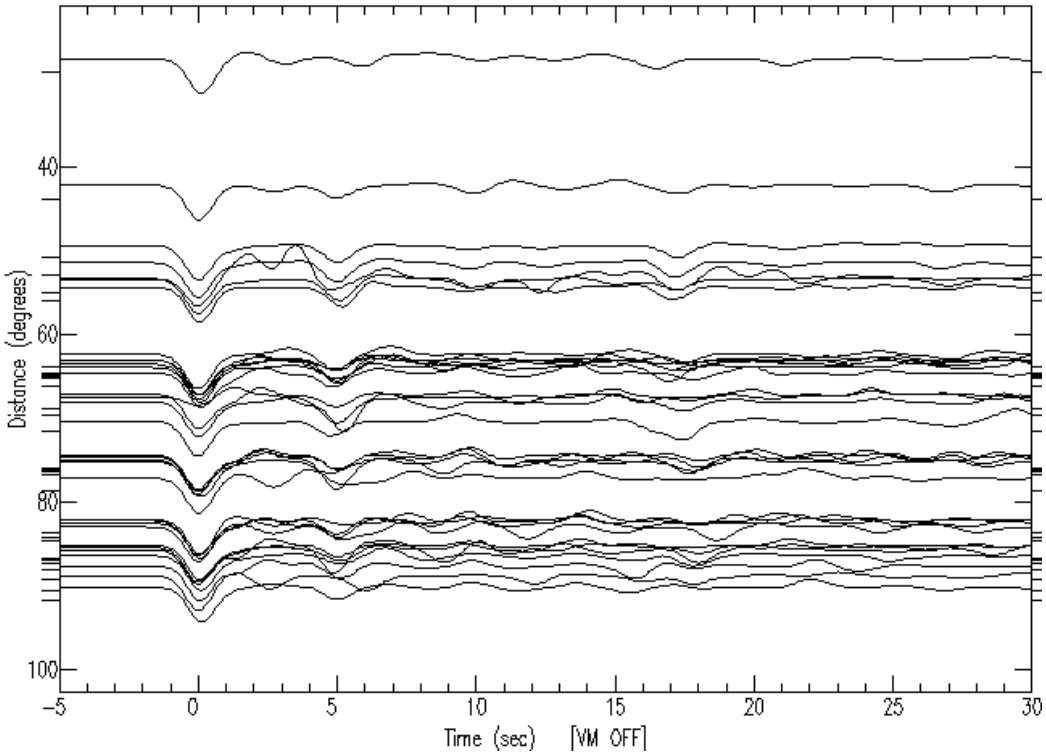

Figure 16 - TROLL stack file list record section plot

Through visual inspection, it is evident that some of the receiver functions do not conform nicely with the rest. Such receiver functions were identified and removed from the stack file list. An example of a poor fitting receiver function is illustrated in Figure 17. In this example, the receiver function of the blue event does not coincide well with the other events, and it is consequently removed from the stack file list. After cleaning, the stack file list of TROLL had 30 events and the stack file list of SNAA had 164 events. The cleaned stack file list for SNAA is plotted in Figure 18.

-

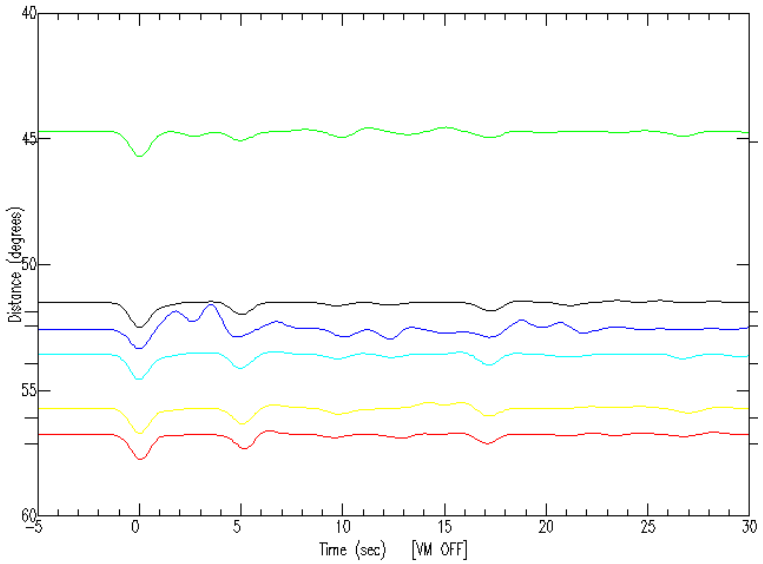

Figure 17 - Close up of the TROLL stack file list record section plot. The blue event is considered to have poor coincidence with the other events, and should therefore be removed.

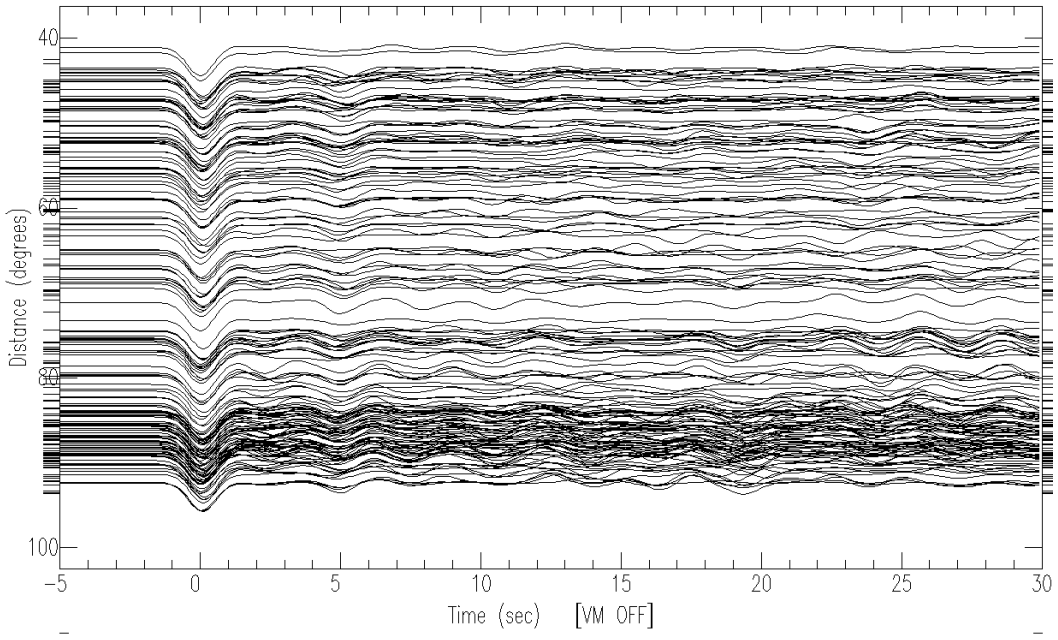

Figure 18 - A cleaned SNAA stack file list record section plot

Once the stack file list is considered cleaned for outliers or contaminating receiver functions, a summation of the stacks can be performed. The command *sumstack* is used to stack all the traces in the stack file list. Through this process, a moveout correction is applied to each trace by shifting the signal in accordance with its static and dynamic delays, and all the signals are summed into a single trace (Figure 19 and Figure 20). The resulting summated stack serves as the overall observed receiver function for the remaining subsurface modeling procedures.

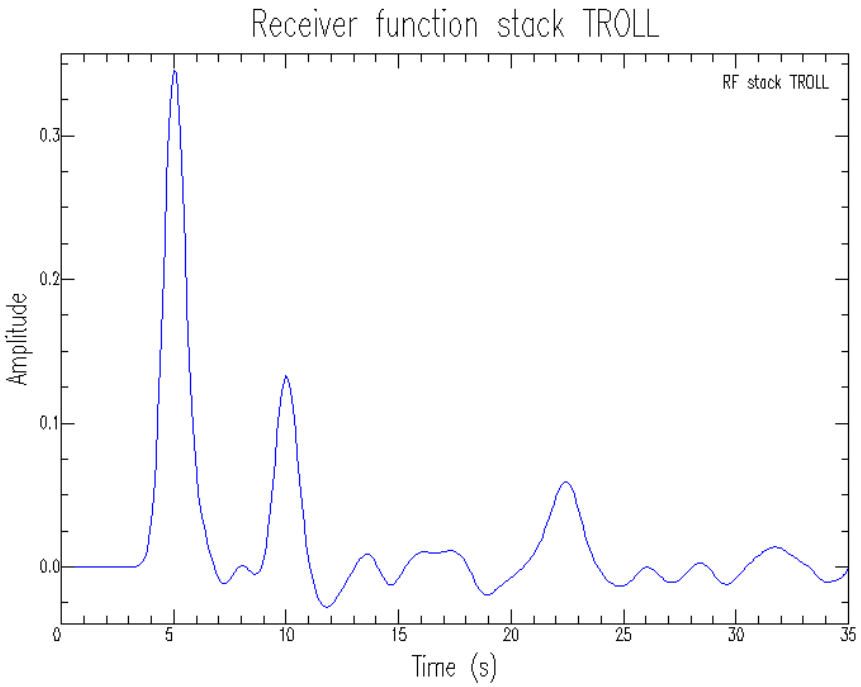

Figure 19 - Summated stack of TROLL receiver functions

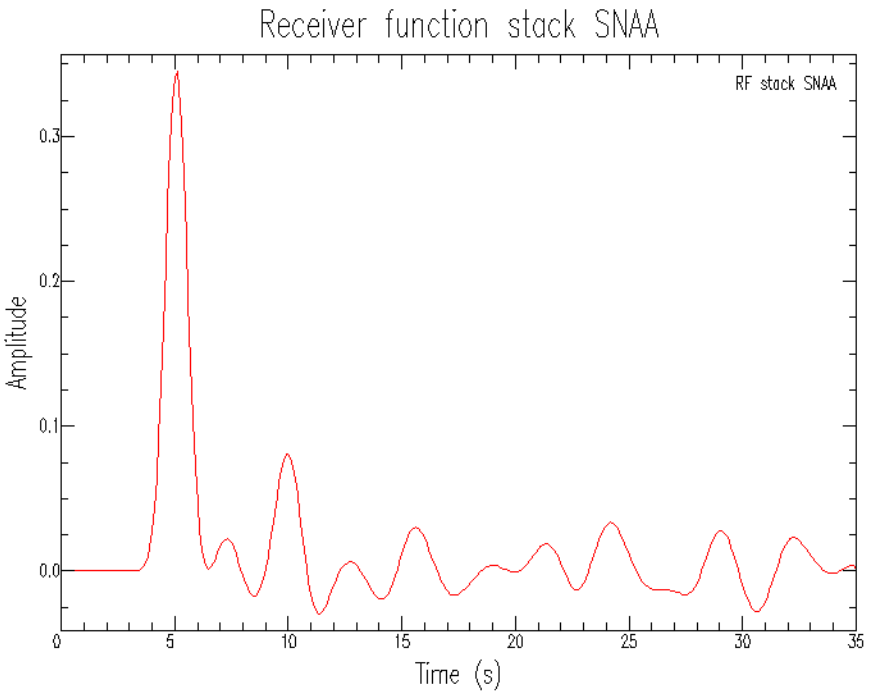

Figure 20 - Summated stack of SNAA receiver functions

By visual inspection of the resulting receiver function stacks (Figure 19 and Figure 20), it is apparent that the receiver function for TROLL has better defined signal peaks of the generated multiples than the receiver function for SNAA. This may indicate that the structure

-

underneath SNAA is more complex than the one underneath TROLL; thus the modeling of SNAA may prove to be more difficult to model or have a higher inversion misfit than for TROLL.

4.3 H-κ Analysis

The range of slownesses in a typical receiver function study does not appear to be broad enough to remove the depth-velocity ambiguity; the inclusion of a priori information is necessary (Ammon et al., 1990). Therefore, to obtain initial estimates of crustal structure and composition, the H-κ stacking method of Zhu and Kanamori (2000) was used. The technique takes use of the directly arriving P-to-S conversion P_S and the later arriving multiples crustal reverberations (multiples) P_pP_s and $P_pP_s + P_pS_s$, in a stacking algorithm (Figure 4). The goal of the technique is to estimate the crustal thickness (H) and average V_P/V_S ratio (κ) from the receiver function time series. The V_P/V_S ratio, is directly linked to the Poisson ratio (σ), see equation (4), whose properties are known to provide better diagnostics of crustal composition than P- or S-wave data alone (Zandt et al. 1995; Chevrot &van der Hilst 2000).

$$\sigma = \frac{1}{2}\left(1 - \left[\left(\frac{V_P}{V_S}\right)^2 - 1\right]^{-1}\right) \qquad (4)$$

To perform the H-κ analysis, an auxiliary SAC program called *hk* was used (Helffrich, 2006). The objective function for the H-κ stacking technique is shown below:

$$s(H,\kappa) = \sum_{j=1}^{N} w_1 r_j(t_1[H,\kappa]) + w_2 r_j(t_2[H,\kappa]) - w_3 r_j(t_3[H,\kappa]) \qquad (5)$$

N is the number of receiver functions used; w_1, w_2, w_3, are the weights; $r_j(t)$ are the receiver function amplitudes at the predicted arrival time of P_S *(t_1)*, P_pP_s *(t_2)* and $P_pP_s + P_pS_s$ *(t_3)* for receiver function number *j*. The objective function in equation (5) was evaluated for a grid search range between $25 \leq H \leq 50$ km, and $1.5 \leq \kappa \leq 2.0$, with grid lines at 0.05 km and 0.01 increments respectively. The three arrival times are predicted by the following equations:

$$t_1[H,\kappa] = H\left[\sqrt{\frac{\kappa^2}{V_P^2} - p^2} - \sqrt{\frac{1}{V_P^2} - p^2}\right] \qquad (6)$$

$$t_2[H,\kappa] = H\left[\sqrt{\frac{\kappa^2}{V_P^2} - p^2} + \sqrt{\frac{1}{V_P^2} - p^2}\right] \qquad (7)$$

$$t_3[H,\kappa] = 2H\sqrt{\frac{\kappa^2}{V_P^2} - p^2} \qquad (8)$$

V_P is an assumed average P-wave velocity through the crust, and p is the horizontal slowness (s/° or s/km), also called the ray parameter. To estimate the horizontal slowness for each event, the auxiliary SAC program *setrfslow* was used (Helffrich, 2006). The software computes the horizontal slowness based on incidence angle, interpreted P-to-S conversion from the receiver function, and the iasp91 travel time model. The computed horizontal slowness was then written in a user defined variable storage area within the header of each file in units of seconds per kilometer.

As the files now contained the horizontal slowness, the only other value necessary to run the algorithm was an assumed average P-wave velocity. V_P was entered as part of the input for the program and solutions were obtained for multiple values until an ideal solution was found. The ideal solution was considered the solution yielding the minimum amount of RMS error which occurred at average V_P of 6.40 km/s and 6.38 km/s for TROLL and SNAA respectively. The resulting estimations, along with their error values, are shown in table below..

Station	Crustal Thickness (km)	VS/VP ratio
TROLL	42.48 ± 0.85	1.714 ± 0.026
SNAA	38.63 ± 0.63	1.796 ± 0.020

4.3.1 Analysis of TROLL

The results of the H-κ analysis for TROLL is illustrated by a contour plot in Figure 21. The contours represent percentile confidence regions. The solution for the bulk crustal structure estimates falls within the 95% region, yielding a crustal thickness prediction under TROLL to be 42.5 km with and a V_S/V_P ratio of 1.71.

-

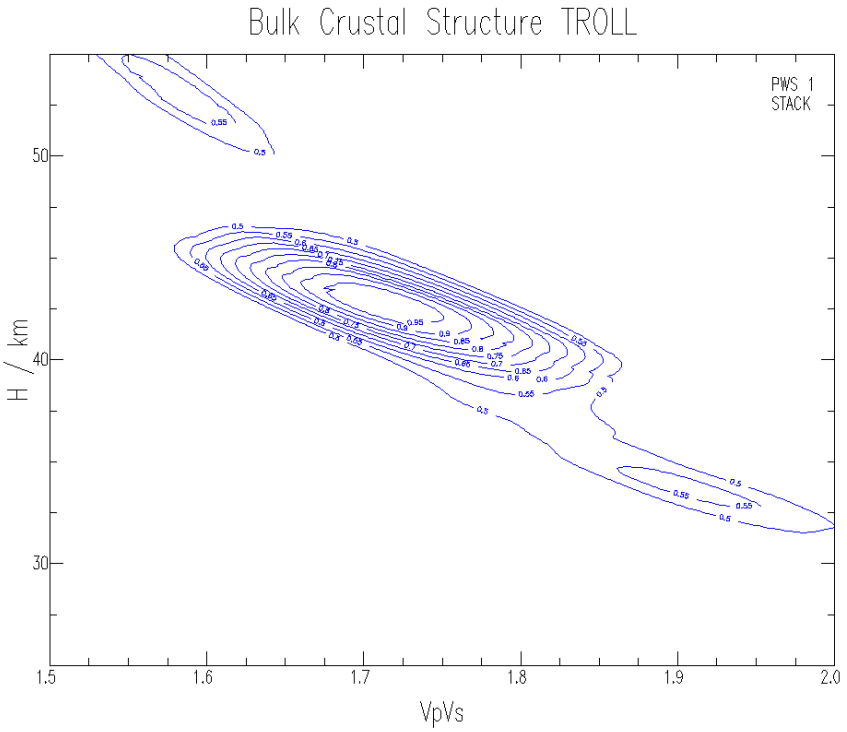

Figure 21 - H vs κ contour plot for TROLL

4.3.2 Analysis of SNAA

A resulting contour plot from the H-κ analysis of SNAA is shown in Figure 22. Somewhat of an ambiguity can be seen this plot compared to that of TROLL; in addition to the solution at crustal thickness 38.6 km and V_S/V_P ratio of 1.79, there is an increased confidence region occurring between a depth of 49 to 55 km depth and V_S/V_P ratio of 1.55 to 1.65. This corresponds well with results found by Bayer et al. (2009) when they performed H-κ analysis for SNAA station as part of a Moho depth study for Queen Maud Land. In their study, two solutions for the crustal parameters were found: (1) crustal thickness of 50 km with a low Vp/Vs ratio of 1.62 (2) crustal thickness 40 km with a higher Vp/Vs ratio of 1.80 (Bayer et. Al, 2009).

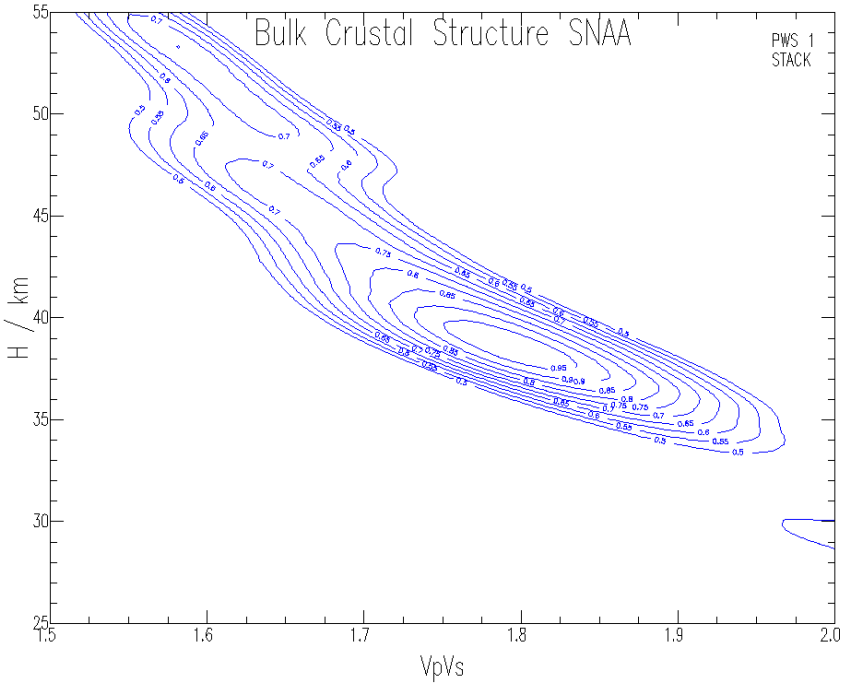

Figure 22 - H vs κ contour plot for SNAA

4.4 Forward Modeling and Inversion

Through forward modelling, a receiver function can easily be determined based on a given earth structure model. The problem of this study however is not to find the receiver function, but rather to determine the earth structure that generate the receiver function; an inverting process. Inversion of a waveform is a data-fitting procedure that aims at obtaining estimates of crustal properties from the receiver function. Given an initial model of the subsurface parameters, the data are predicted by solving a wave-equation. The model is then updated through forward modeling in order to reduce the misfit between the observed and predicted data. This procedure is repeated in an iteratively until the misfit between the model and receiver function data is satisfactorily small.

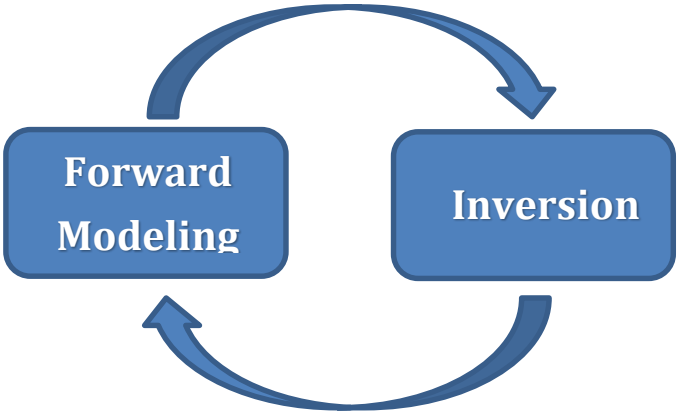

-

4.4.1 Velocity Model

To perform the waveform inversion, an initial model needs to be defined. The receiver function programs of Ligorría and Ammon (1999) takes use of an ASCII velocity model format designed by Tom J. Owens (TJO Model Format). The format has spaces for V_P, V_S, density, thickness, attenuation values for the p and s, strike, dip, and Poisson's ratio, defined for the number of structural intervals desired. The units for the velocities and density is km/s and g/cm^3 respectively. Poisson's ratio in the file is completely determined by the V_P and V_S, and acts as a check to make sure the input velocities has the correct V_P/V_S ratio. The values for the strike, dip and the attenuations are left to as zeros.

A program called *icmod* was used to create an initial velocity model in the TJO format. Thereafter, the model could easily be changed as preferred using an ascii editor.

The estimates acquired through the H-κ analysis was used for the initial models for the analysis of both TROLL and SNAA. The starting velocity model for TROLL was designed with a crustal P-wave velocity of 6.4 km/s, with a sharp discontinuity (8.0 km/s) at the assumed Moho depth 42.5 km. The P- and S-wave velocities were set such that Poisson's ratio was 0.242, which corresponds to a V_P/V_S ratio of 1.714. In the case of SNAA, the P-wave velocity was the same (6.4 km/s), while the S-wave velocity was changed with accordance to a V_P/V_S ratio of 1.796 ($\sigma = 0.275$), and the Moho discontinuity was set shallower at a depth of 38.6 km.

4.4.2 Waveform Inversion

The waveform inversion programs includes *snglinv* and *smtinv*. Both programs execute a linearized, iterative inversion of a specified waveform, and incorporates a minimum roughness constraint to remove non uniqueness problems from each individual inversion (Ammon, 1997). Partial derivatives are calculated using a finite-difference approximation using efficient algorithm codes by George Randall (1989, 1994) whose work is based on the intricacies of Kennett's (1983) reflection-matrix approach to seismogram computation.
The inversion computation for both programs are similar, *snglinv* is predominately used to estimate the number of iterations required, while *smtinv* which is used fit the best smoothing parameter. Through testing, a number of ten iterations and a smoothness trade-off parameter of 0.4 was selected to achieve a final model. The inversion requires a horizontal slowness value. As the epicentral distance interval for event picking was between 30° to 95°, the average

distance 62.5° was used to get a horizontal slowness value of 6.7 s/° from IASPEI (1991). The program requires the unit to be seconds per kilometer, so the value was converted; 0.06 s/km was used as input. For the initial inversion, a high layer discretization was used; layers of 1 km thickness. The resulting P-wave velocity models from this inversion are shown for both TROLL and SNAA in Figure 23. From the models, it is apparent that the subsurface under SNAA is more complex than that off TROLL. These are initial models, with purpose to give an idea of the structural developments. Through the continued processing, the goal is to minimize the number of layer discretization and find the smoothest model matching the observations.

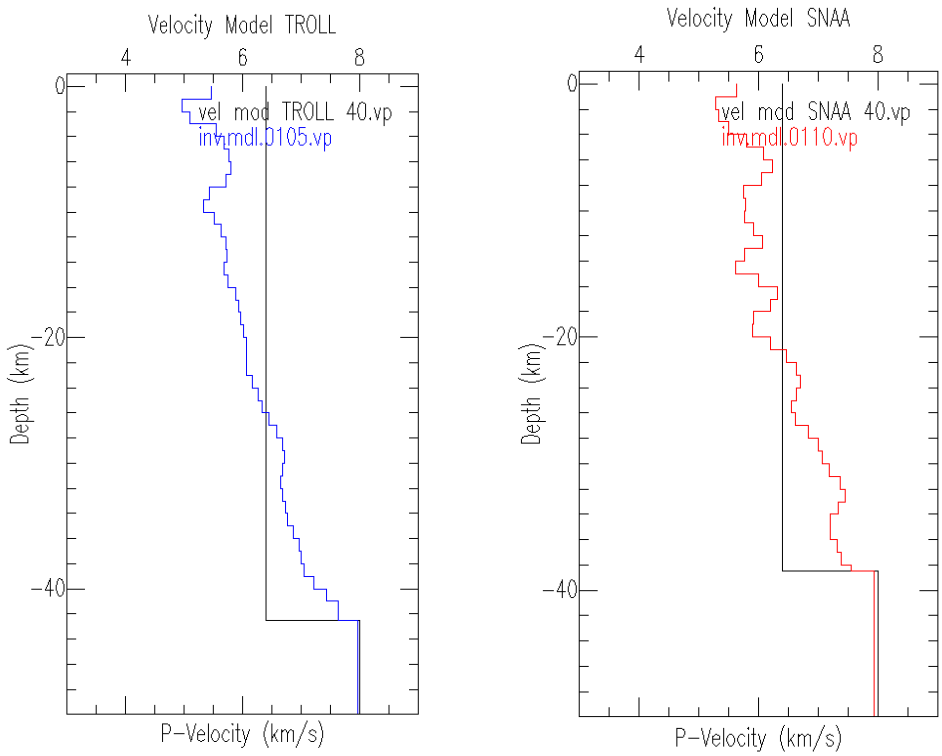

Figure 23 - P-wave velocity model for TROLL (Left). P-wave velocity model for SNAA (Right)

Through an interactive iterative process, solutions from the waveform inversions were evaluated before making optimizing changes to the initial data. The evaluation was performed both visually and numerically; by viewing the resulting velocity model and its synthetic seismic, along with the percentage of misfit calculated between model and receiver function data. Adjustments were then done to the initial velocity model by modifying the layer discretization and thicknesses in an attempt to improve the inversion results.

The final, optimized solution for TROLL is illustrated in Figure 24. The blue seismogram is the receiver function stack from observations, and the red seismogram is the resulting waveform from the inversion. As anticipated from the stacked receiver functions (4.2), the optimized inversion of TROLL had a lower misfit compared to SNAA, as SNAA is expected to have more

-

complex subsurface structures. The resulting velocity models are further discussed in the next chapter.

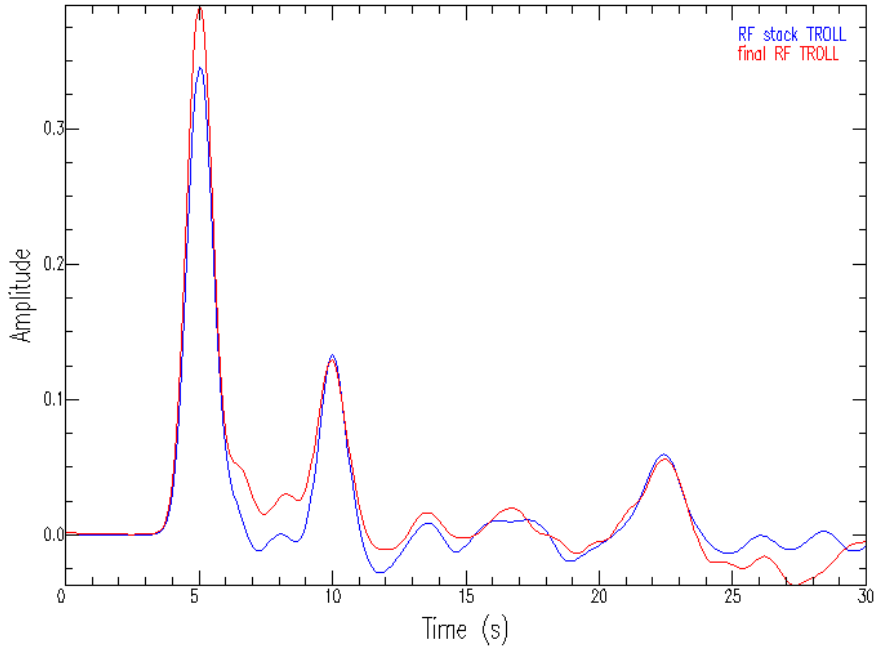

Figure 24 - The summated stack receiver frunction (blue) plotted against the resulting waveform from inversion (red).

5 Results

5.1 TROLL

The subsurface parameter values for the final inversion results for the subsurface model underneath TROLL seismic station are shown in the table below.

Layer	Depth (km)	Thick-ness (km)	V_P (km/s)	V_S (km/s)	Density (g/cm^3)	σ
1	3.0	3.0	5.12	2.99	2.41	0.242
2	4.0	1.0	5.44	3.17	2.51	0.242
3	8.0	4.0	5.54	3.23	2.54	0.242
4	10.0	2.0	5.38	3.14	2.49	0.242
5	12.0	2.0	5.59	3.26	2.56	0.242
6	16.0	4.0	5.78	3.37	2.62	0.242
7	18.0	2.0	5.90	3.44	2.66	0.242
8	24.0	6.0	6.03	3.52	2.70	0.242
9	26.0	2.0	6.26	3.65	2.77	0.242
10	33.0	7.0	6.46	3.77	2.84	0.242
11	36.0	3.0	6.61	3.86	2.88	0.242
12	39.0	3.0	6.82	3.98	2.95	0.242
13	40.0	1.0	7.09	4.13	3.04	0.242
14	41.0	1.0	7.33	4.28	3.12	0.242
15	42.5	1.5	7.56	4.41	3.19	0.242

The resulting S-wave velocity model of from the parameter values is shown in Figure 25.

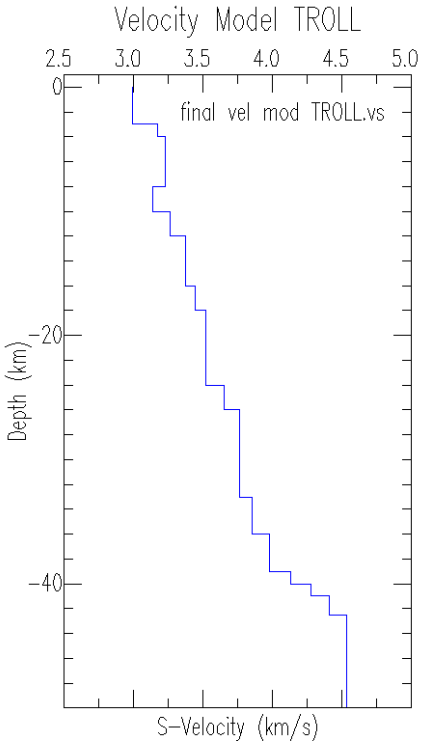

Figure 25 - S-wave velocity model for TROLL

-

The corresponding receiver function for the final model solution of TROLL is illustrated in the plot below (Figure 26)

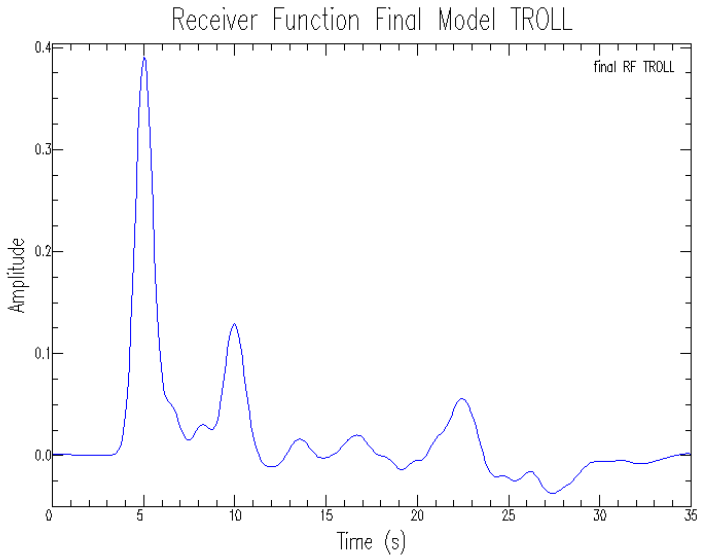

Figure 26 - The resulting receiver function waveform for the final model solution of TROLL

5.2 SNAA

Below is a table with the subsurface parameter values for the final inversion results for the crustal model underneath SNAA seismic station..

Layer	Depth (km)	Thick-ness (km)	V_P (km/s)	V_S (km/s)	Density (g/cm^3)	σ
1	2.0	2.0	5.27	2.93	2.46	0.275
2	4.0	2.0	5.57	3.10	2.55	0.275
3	5.0	1.0	5.77	3.21	2.62	0.275
4	8.0	3.0	5.90	3.29	2.66	0.275
5	10.0	2.0	5.70	3.17	2.59	0.275
6	11.0	1.0	5.84	3.25	2.64	0.275
7	16.0	5.0	6.09	3.39	2.72	0.275
8	22.0	6.0	6.40	3.57	2.82	0.275
9	24.0	2.0	6.69	3.72	2.91	0.275
10	31.0	7.0	6.93	3.86	2.99	0.275
11	38.6	7.6	7.27	4.05	3.10	0.275

S-wave velocity model for the subsurface underneath SNAA is shown in Figure 27.

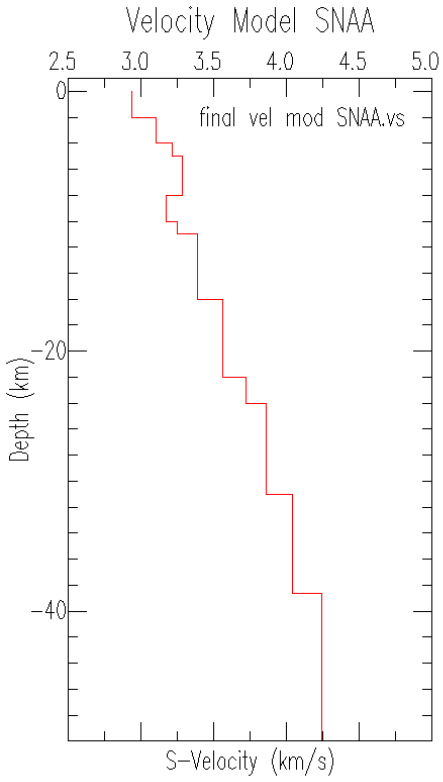

Figure 27 - S-wave velocity model for SNAA

The corresponding receiver function for the final model solution of SNAA is illustrated in the plot below (Figure 28)

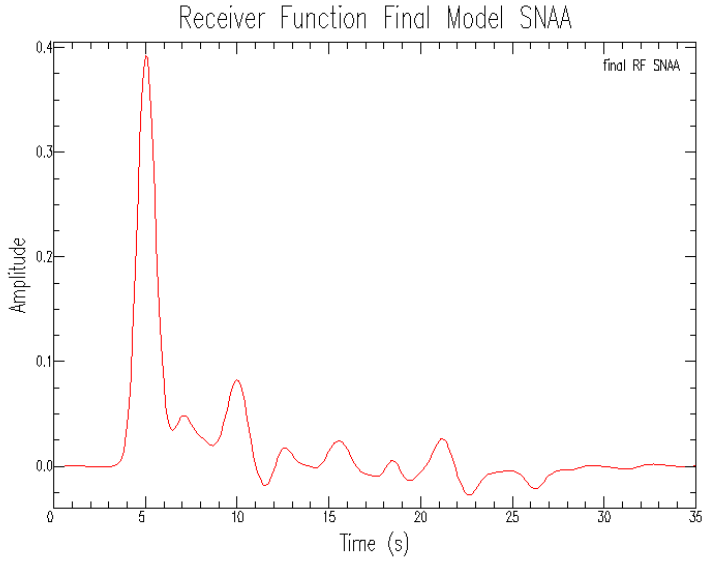

Figure 28 - The resulting receiver function waveform for the final model solution of SNAA

-

6 Discussion

6.1 Comparison of TROLL and SNAA

6.1.1 Velocity models and crustal structure

The P-wave velocity model for TROLL and SNAA are plotted together in Figure 29. The general trend of the models behaves very similarly, and since the two seismic stations are relatively close to each other, this similarity of velocity models indicates relating subsurface structures. At a depth of around 8 to 11 km, both models encounter a zone of lower velocity. A study by Zollo et al., (1996) suggests that such low-velocity layers might correspond to sedimentary strata overthrust by sheets of crystalline rocks. As mentioned in the geological setting section (1.1), the mountain ranges in Queen Maud Land is believed to be composed of cambrian crystalline and granite. This presence of crystalline may explain this low velocity zone.

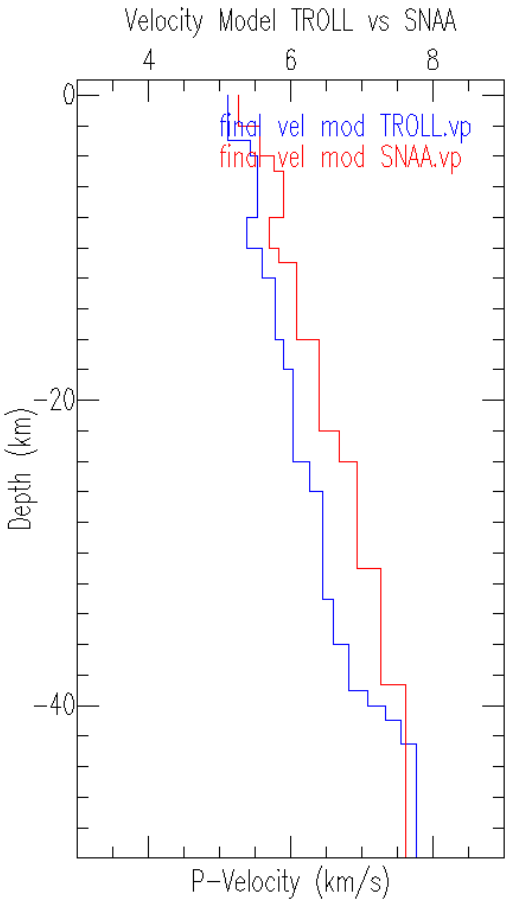

Figure 29 - Comparison of the P-wave velocity models for TROLL (blue) and SNAA (red)

Continuing to greater depths, the trend for both models remain similar, with the difference being that significant changes are occurring at slightly deeper depths for TROLL than for SNAA. This thickness difference continues to grow rather linearly until both models reach their respective estimated Moho depths. The velocity difference remain rather constant until a depth of about 22 km, at which the velocity difference begin increase. This suggests relatively similar composition until at this depth, and that significant compositional changes occur at depths below 22 km. The estimated average Poisson's ratio SNAA is relatively high, 0.275 ($V_P V_S$ ratio of 1.796), and may be an indication of more mafic material in this region than in the region underneath TROLL (Bayer et al., 2009).

6.1.2 Moho depth

Comparing the receiver functions of TROLL and SNAA (Figure 30), one can clearly see that the responses caused by multiples arrive earlier for SNAA than for TROLL; suggesting that the Moho depth for SNAA is shallower than for TROLL. Therefore, it is no surprise that the

-

H-κ analysis which bases its algorithms on the arrival time of the multiples, yielded a thicker crust estimate for TROLL than for SNAA : TROLL, 42.5 km, and SNAA, 38.6 km.

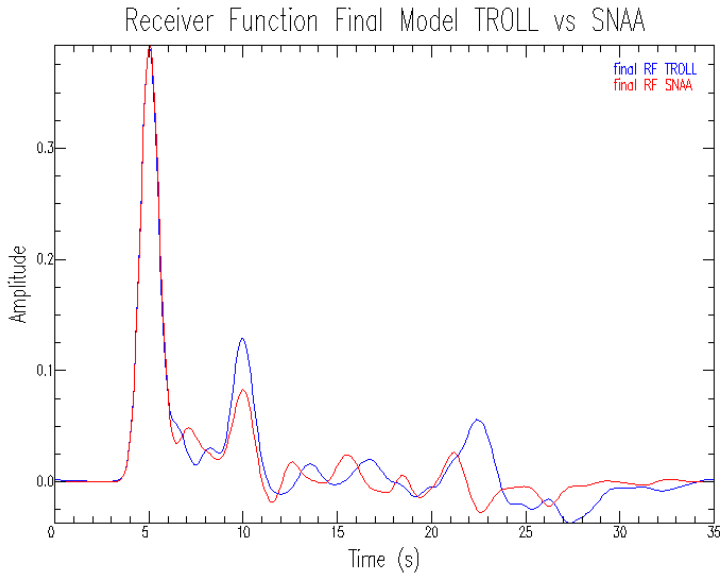

Figure 30 - Comparison of the receiver functions of the final models of TROLL (blue) and SNAA (red)

Furthermore, there is a clear correlation worldwide between continental elevation and crustal thickness. The crust can be seen as "floating" on the mantle. As any floating object, the thicker the object is, the longer it will extend in both elevation and depth relative to the material it is floating in. In other words, the crust-mantle boundary is expected to be located deeper under regions of higher elevations than in regions of lower elevation. The TROLL station is located at more than 550 m higher elevation than the SNAA station (1399 m and 846 m respectively), and a higher continental elevation implies thicker the crust as explained above. This further strengthens the confidence in the results obtained from the receiver function method.

6.1.3 Numerical errors

The SNAA seismic station has been operational since 1997, while the TROLL seismic station began its recordings in 2012. Naturally, SNAA would most certainly have more useable events. This higher number of observation for SNAA explains why the resulting error-estimates of the H-κ analysis are lower for SNAA than TROLL. This makes sense numerically as SNAA has higher redundancy, but does not necessarily mean more trust should be given to the final structural model of SNAA. The subsurface underneath SNAA appears to be more complex than that underneath TROLL, thus the final model for TROLL may be considered a more accurate

estimate than the one for SNAA. The numerical misfit values from the inversion further strengthens this claim, as the inversion of TROLL had lower misfit compared to SNAA.

6.2 The number of events

Through the various processing steps, a considerable amount of the events are deemed unfit to be included in the analysis. The number of events kept after each step in the receiver function analysis process is shown in the table below.

Process	Events TROLL #	Events SNAA #
Event search	154	685
Event extraction	94	400
Deconvolution	34	171
Stacking	30	164

In particular, a large number of events are lost in the deconvolution step for source equalization. This is due to the strict criteria of only keeping receiver functions generated with a reproduction of 90% of the signal. The criteria could have been lowered to 80%, which still generates decent receiver functions, but to not compromise the quality to get more observations, the strict criteria was kept. Another possible reason why such a large fraction of the events was deemed unfit during this process is that process, contrary to the preceding, involved numerical evaluations, whereas the preceding process involved visual evaluations of seismograms performed by an inexperienced operator.

-

7 Conclusion

The main purpose of this study was to determine the crustal thickness underneath the TROLL seismic station on Queen Maud Land through the technique of receiver function modeling. The closest neighboring seismic station SNAA was used to compare and evaluate the results obtained for TROLL. Comparison between the two indicates relating subsurface structures. To further evaluate whether the thickness results are plausible, the results are here compared to estimates generated through other studies. Crustal depths from previous refraction studies by Kudryavtzek et al. (1991), Kogan (1992), Jokat et al. (2004), and Bayer et al. (2009) are shown in the illustration below (Figure 31). On the illustration, the location of the TROLL seismic station is approximated by a red triangle. This study yielded an estimated Moho depth of 42.5 km below TROLL. Comparison of this value with the surrounding depth estimates further strengthens the confidence in the estimate solution. If one estimate a linear vertical trend drawn between SNAA (40 km) and the WM-stations on the Wohlthat Massiv (47 to 50 km), a depth value around 42.5 km seems highly plausible.

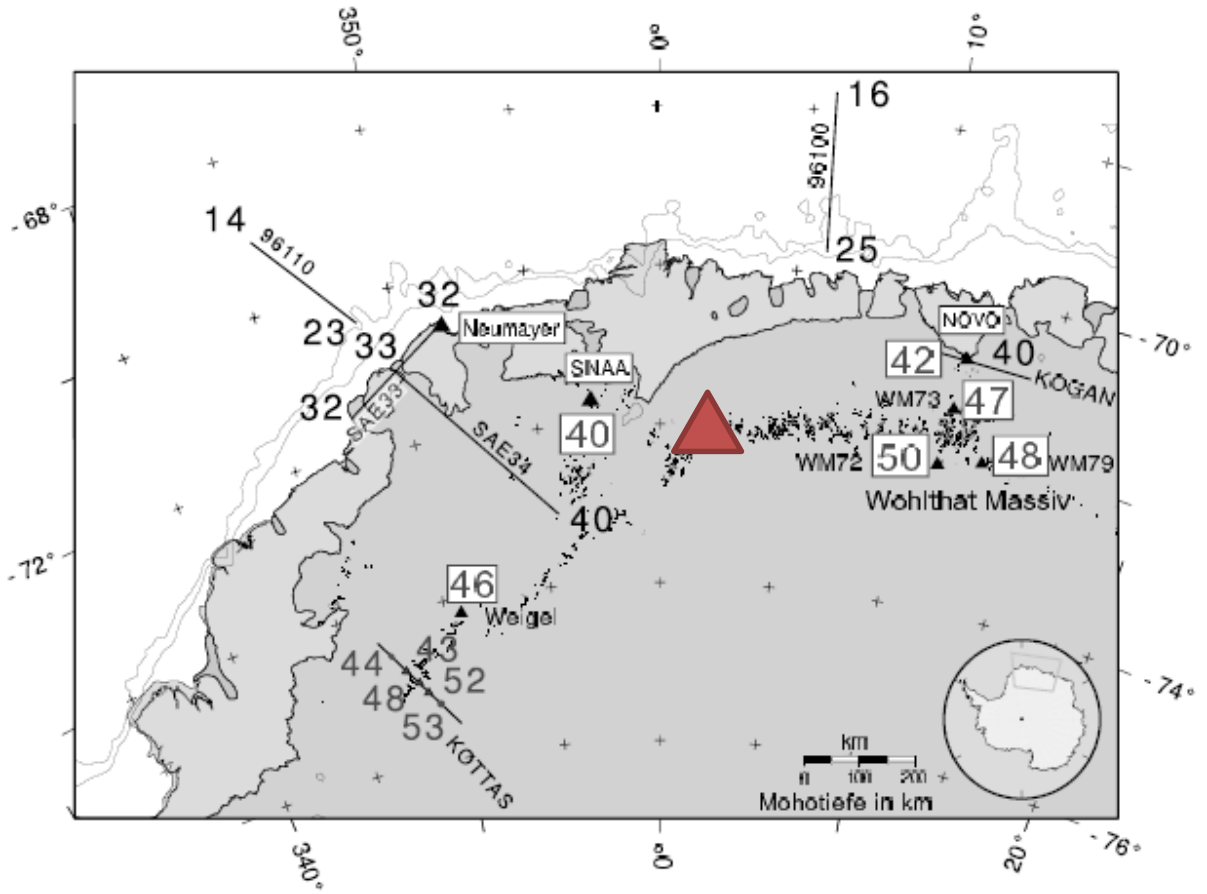

Figure 31 - Map of Queen Maud Land with crustal thickness estimates from previous studies (Courtesy of Bayer et al., 2009).

References

Ammon, C. J., The isolation of receiver effects from teleseismic P waveforms, Bull. Seism. Soc. Am., 81, 2504-2510, 1991.

Ammon, C. J., G. E. Randall and G. Zandt, On the non-uniqueness of receiver function inversions, J. Geophys. Res., 95, 15303-15318, 1990.

Ammon, C. J., and G. Zandt, The receiver structure beneath the southern Mojave Block, Bull. Seism. Soc. Am., 83, 737-755, 1993.

Ammon, C.J., http://eqseis.geosc.psu.edu/~cammon/HTML/RftnDocs/rfinv01.html, accessed 2015, published 1997.

Bayer, Bettina; Geissler, Wolfram H.; Eckstaller, A.; Jokat, Wilfried: Seismic imaging of the crust beneath Dronning Maud Land, East Antarctica. Geophysical Journal International 178.2, 2009.

Chevrot, S. & van der Hilst, R. D.,The Poisson ratio of the Australian crust: Geological and geophysical implications, Earth and Planetary Science Letters, 183(1-2), 121–132, 2000.

Clayton, R. W., and R. A. Wiggins, Source shape estimation and deconvolution of teleseismic body waves, Geophys. J. R. Astron. Soc., 47, 151-177, 1976.

Elliot, D, H., 1991. Triassic-Early Cretaceous evolution of Antarctica. In: Thomson, M.R.A.. Crame, J. A. and Thomson, J. W. (Eds.) Geological Evolution of Antarctica. Cambridge University Press, Cambridge, England,: 542-548

Elvevold, Synnøve, http://www.polarhistorie.no/filearchive/Faktaark_NP_012.pdf, accessed 2015, published 2005

Gjeldsvik, Tore, Dronning Maud Land. I Store norske leksikon, 2009 https://snl.no/Dronning_Maud_Land, accessed 2015.

-

Helffrich, George. Extended-time multi-taper frequency domain cross-correlation receiver function estimation. Bull. Seismo. Soc. Am., v. 96, 344-347, 2006.

Helffrich, GR, Wookey, JM & Bastow, ID, 'The Seismic Analysis Code: A Primer and User's Guide'. Cambridge University Press, 2013.

IASPEI 1991, Kennett, B.L.N. (Compiler and Editor),Seismological Tables, Bibliotech, Canberra, Australia, 167 pp., 1991.

International Seismological Centre, On-line Bulletin, http://www.isc.ac.uk, Internatl. Seis. Cent., Thatcham, United Kingdom, accessed 2015.

Jacobs, J., Bauer, W., Spaeth, G., Thomas, R.J. & Weber, K.: Lithology and structure of the Grenville-aged (~1.1 Ga) basement of Heimefrontfjella (East Antarctica).- Geol. Rundsch. 85: 800-821, 1996.

Jacobs, J., Fanning, C.M., Bauer, W., Timing of Grenville-age vs. Pan-African medium- to high grade metamorphism in western Dronning Maud Land (East Antarctica) and significance for correlations in Rodinia and Gondwana, 2003.

James Stewart Monroe; Reed Wicander, The changing Earth: exploring geology and evolution (5th ed.). Cengage Learning. p. 216. ISBN 0-495-55480-4, 2008.

Jokat, W., Ritzmann, O., Reichert, C., & Hinz, K., Deep crustal structure of the continental margin off the Explora Escarpment and in the Lazarev sea, East Antarctica, Marine Geophysical Researches, 25(3-4), 283–304, 2004

Kaul M. K., Singh R. K., Srivastava D., Jayaram S., Mukerji S., Petrographic and structural characteristics of a part of the East Antarctic Craton, Queen Maud Land, Antarctica. International Symposium on Antarctic Earth Sciences 5: 89-94, 1991.

Kennett, B. L. N., Seismic Wave Propagation in Stratified Media, Cambridge University Press, Cambridge, England, 342 pages, 1983.

Kogan, A. L., Results of deep seismic sounding of the Earth's crust in East Antarctica, in Antarctic Geology and Geophysics, edited by R. Adie, pp. 485–489, 1992

Kudryavtzek, G., Butzenko, V., & Kadmina, I., Crustal section across western Dronning Maud Land continental margin from geophysical data, in Abstracts, Sixth international symposium on Antarctic earth science, pp. 330–335, National Institute for Polar Reasearch, Tokyo, 1991.

Ligorria, J. P., and C. J. Ammon, Iterative deconvolution and receiver-function estimation, Bull. Seismol. Soc. Am.,89, 1395–1400, 1999.

Midzi, V. and L. Ottemöller, Receiver function structure beneath three Southern Africa Seismic broadband stations, Tectonophysics, 339, 443-454, 2001

Minoo, Kosarian, Lithospheric structure of north Africa and western Eurasia,The Pennsylvania State University; Publication Number: AAI3343694; ISBN: 9780549991816; Source: Dissertation Abstracts International, Volume: 70-01, Section: B, page: 0176.; 333 p, 2006.

Mohorovičić, A. Das Beben vom 8 x 1909, Jahrbuch des Meteorologischen Observatoriums in Zagreb Fur das Jahr 1909 9, 1-63, 1909.

Norwegian Polar Institute, http://www.npolar.no/en/the-antarctic/dronning-maud-land.html, accessed 2015.

Plešinger, A., M. Hellweg and D. Seidl, Interactive high-resolution polarization analysis of broadband seismograms. J. Geophysics, 59, p. 129-139, 1986.

Randall, G. E., Efficient calculation of differential seismograms for lithospheric receiver functions, Geophys. J. Int., 99, 469-481, 1989

Randall, G. E., Efficient calculation of complete differential seismograms for laterally homogeneous earth models, Geophys. J. Int., 118, 245-254, 1994.

Rondenay, Stéphane, Upper Mantle Imaging with Array Recordings of Converted and Scattered Teleseismic Waves Stéphane Rondenay Published online: 8 May 2009 Springer Science+Business Media B.V. 2009

Schweitzer, J., Pirli, M., Roth, M., Kværna, T., TROLL – a new, very broadband seismic station in Antarctica, NORSAR Scientific Report No. 1-2013, Kjeller, 2013

-

Trabant, Chad https://seiscode.iris.washington.edu/projects/mseed2sac/wiki, accessed 2015, published 2013.

USGS, http://earthquake.usgs.gov/learn/glossary/?termID=150, accessed 2015.

Zandt, G., and C. J. Ammon, Continental Crustal composition constrained by measurements of crustal Poisson's ratio, Nature, 374, 152-154, 1995.

Zhu, L. & Kanamori, H., 2000. Moho depth variation in southern California from teleseismic receiver functions, Journal of Geophysical Research B: Solid Earth, 105(B2), 2969–2980.

Zollo, A. Gasparini, P., Virieux, J., Le Meur, H., de Natale, G., Biella, G., Boschi, E., Capuano, P., de Franco, R., dell'Aversna, P., de Matteis, R., Guerra, I., Iannaccone, G., Mirabile, L., Vilardo, GSeismic Evidence for a Low-Velocity Zone in the Upper Crust Beneath Mount Vesuvius, Science, Volume 274, Issue 5287, pp. 592-594, 1996